RSC Advances

ROYAL SOCIETY OF CHEMISTRY

www.rsc.org/advances

Stark sublevels in Tm^{3+}-Yb^{3+} codoped $Na_2Y_2B_2O_7$ nanophosphor for multifunctional applications

Abhishek Kumar Soni, Riya Dey, Vineet Kumar Rai*

Laser and Spectroscopy Laboratory

Department of Applied Physics

Indian School of Mines, Dhanbad-826004

Jharkhand, India

* Authors to whom correspondence to be made:

Email address: vineetkrrai@yahoo.co.in; rai.vk.ap@ismdhanbad.ac.in

Phone No. - +91-0326-2235404

Abstract

Phase and crystal structure of the $Na_2Y_2B_2O_7$:Tm^{3+}-Yb^{3+} inorganic phosphor prepared by solution combustion method has been identified by powder X-ray diffraction technique. Surface morphology and particle size has been examined by using the field emission scanning electron microscopy and high resolution transmission electron microscopy characterizations of the prepared materials. No absorption band around 980 nm has been observed in the Tm^{3+} doped phosphors, whereas a broad band around 980 nm in the Tm^{3+}-Yb^{3+} codoped phosphors corresponding to the $^2F_{7/2} \leftarrow ^2F_{5/2}$ absorption transition of Yb^{3+} ion has been detected. The upconversion emission bands have been observed in the UV, visible and NIR regions upon excitation with 980nm laser diode. The temperature sensing behaviour and the concept of nanoheater in the developed nanophosphor has been demonstrated by using the stark sublevels of the $^1G_4$ level of Tm^{3+} ion, which is responsible for the blue upconversion emission. The maximum sensor sensitivity of about 4.54×10^{-3} K^{-1} at 300 K for the developed multifunctional nanophosphor has been determined. The temperature gain of about ~435 K has been observed at laser power density of 66.88 W/cm^2 and the colour coordinates do not change with the variation of pump power density. For localizing and heating the hyperthermia based cancer cells by using the NIR radiation a very low pump power density of about ~7.0 W/cm^2 has been established. The experimental observations prove the developed material to be used as a multifunctional nanomaterial in optical devices and biological applications.

Keywords: *Rare earth, upconversion, nanophosphor, colour coordinate, temperature sensor, nanoheater.*

1. Introduction

The phosphors doped with rare earth (RE) ions are very attractive for many applications, namely in the field of display devices, temperature sensor, optical nanoheater, solar cell efficiency enhancement, bio-imaging, fingerprint detection [1-6]. For preparation of the good phosphors (luminescent materials) doped with RE ions, the selection of host material is a very crucial factor to be considered. Therefore, much effort has to be spent on the synthesis and characterization of the solid materials. The researchers are still looking for suitable luminescent materials for different applications based on the upconversion. The photon upconversion (UC) is basically a nonlinear optical effect in which two or more low energy (NIR) photons are used to generate high energy photon [7]. For the growth of good quality UC based phosphor materials researchers have tried to incorporate different combinations of RE ions in suitable hosts [8-11]. The complex inorganic phosphor is capable of producing efficient luminescence and creating the new field for spectroscopic based various optical studies [9, 12]. Recently, the attention has been attracted towards a new complex inorganic host $Na_2Y_2B_2O_7$ for the development of RE doped phosphor materials. The $Na_2Y_2B_2O_7$ is a low phonon frequency (~ 500 cm^{-1}) host having an iso-structure of $Na_2Gd_2B_2O_7$ phosphor [11, 13]. Additionally, $Na_2Y_2B_2O_7$ facilitates all the triply ionized RE ions for the doping purposes and has been used as an excellent luminescence productive host [14]. There is a tremendous demand for getting the improved luminescence in RE doped phosphors based on the choice of activator and a suitable sensitizer. Among the sensitizers, ytterbium ion serves as an admirable and most effective sensitizer in various oxides and halides based host materials [15-17].

In recent years, the optical temperature sensing study by using the RE doped phosphors with the help of thermally coupled levels has become a very interesting objective. The radiation emitted from the thermally coupled levels upon excitation with suitable wavelength can be used to sense the temperature accurately. According to Boltzmann distribution law the temperature can affect the population of certain level as well as the upper energy levels. The fluorescence intensity ratio (FIR) and fluorescence lifetime (FL), techniques are the most excellent promising approach for temperature sensing [18]. The fluorescence intensities arising from two thermally coupled energy levels from the similar RE ions can be used in optical thermometry. Since any small change in the fluorescence intensity arising due to the transition from higher level to lower level depends upon the population of particular level and hence the rate of spontaneous emission transition. Therefore, in the case of thermometric measurement the FIR technique is applicable, as the population of individual two close thermally coupled levels is directly proportional to the total population [19].

The temperature sensing behaviour by using the FIR technique in a group of RE ions viz. Ho^{3+}/Yb^{3+}, Tm^{3+}/Yb^{3+}, Er^{3+}/Yb^{3+} with thermally coupled levels have been reported by several workers [1, 20, 21]. Not only the two closely spaced thermally coupled levels but it has been possible to apply the FIR technique for stark sublevels of a level to monitor the temperature [20, 22]. When the RE ion is incorporated in a host material the energy level of the rare earth ion is generally splitted into number of sublevels due to the ligand field/crystal field. These sublevels are known as the stark sublevels. The current challenges in the optical temperature sensing are to synthesize the luminescent materials by using better and cost effective chemical approaches. The developed material should work in a wide temperature range with higher temperature sensitivity and high accuracy. In case of the thermally coupled energy levels the FIR is independent of the excitation power fluctuations, spectrum losses, and electromagnetic compatibility problem, etc. [23, 24]. In the FIR technique, the optical

temperature sensors utilize the light signals coming at a distance from the objects or sources to measure the temperature [23].

The novel materials that could be useful to generate heat in their nano or micro scale structure, known as 'optical nanoheater', on the excitation of NIR laser sources have been reported by different researchers, which are promising in hyperthermia, drug delivery and cancer treatment applications [21, 25-27]. The NIR excitation has some advantages over other excitation sources such as small light scattering, less damaging to cell, deep penetration capability, high signal to noise ratio for biological studies and clinical applications [1, 28]. To the best of our knowledge no one has reported the frequency upconversion, temperature sensing and optical nanoheater based on the stark sublevels of the $^1G_4$ level of Tm^{3+} ion responsible for blue UC emission band in the Tm^{3+}-Yb^{3+} codoped $Na_2Y_2B_2O_7$ phosphor till date.

The present work describes the synthesis and characterization of the Tm^{3+}-Yb^{3+} codoped $Na_2Y_2B_2O_7$ phosphor prepared by solution combustion method. The effect of codoping with Yb^{3+} ions on the upconversion emissions from the $Na_2Y_2B_2O_7$:Tm^{3+} phosphor upon excitation at 980 nm has been studied. The temperature sensing behaviour and optical heating produced on increasing the excitation power density by using the fluorescence intensity ratio technique has been reported. The effect of pump power density on the colour emitted from the codoped phosphor has also been demonstrated.

2 .Materials and Method

2.1. Phosphor preparation

The Tm^{3+}/Tm^{3+}-Yb^{3+} doped/codoped $Na_2Y_2B_2O_7$ phosphors have been synthesized by using the solution combustion method. The starting raw materials, namely, Y_2O_3, H_3BO_3, Na_2CO_3, Tm_2O_3 and Yb_2O_3 (all 99.9 % pure) were taken. The inorganic $Na_2Y_2B_2O_7$ phosphors were prepared according to the following chemical reactions,

$$2Y_2O_3+8HNO_3 \rightarrow 4Y(NO_3)_2+4H_2O+O_2\uparrow$$

$$4H_3BO_3+8HNO_3 \rightarrow 4B(NO_3)_2+10H_2O+ O_2\uparrow$$

$$Na_2CO_3+2HNO_3 \rightarrow 2NaNO_3+CO_2\uparrow+H_2O$$

$$4Y(NO_3)_2+4B(NO_3)_2+4NaNO_3 \rightarrow 2Na_2Y_2B_2O_7+20NO_2\uparrow+3O_2\uparrow$$

The compositional equations used for the synthesis of the series of samples were as follows,

$$(100\text{-}x)\ Na_2Y_2B_2O_7 + x\ Tm_2O_3$$

where x=0.1, 0.4, 0.8, 1.2 wt.%.

and $$(100\text{-}x\text{-}y)\ Na_2Y_2B_2O_7 + x\ Tm_2O_3 + y\ Yb_2O_3$$

where x=0.4 wt.% and y=0.5, 1.0, 2.0, 3.0, 4.0 wt.%.

The nitrates of all the oxides were obtained by dissolving the raw materials in concentrate nitric acid (HNO_3). The formed nitrates obtained by the stoichiometric amounts of the precursor materials were mixed with urea as reducing fuel in the 1:3 ratio. The mixture (nitrate solution + urea solution) was stirred for 3 hours at 1000 R.P.M at 70^0C. After continuous stirring of the mixtures a transparent homogeneous gel was formed. The formed gel was then transferred into an alumina crucible and placed inside an electrical furnace preheated at 650^0C. The combustion took place and finally dry fluffy mass like as-synthesize samples were produced. The as-synthesized samples were taken out and grinded by using an agate mortar to get uniform fine power. Finally, the as-synthesized samples were annealed at

high temperature at 800^0C for three hours. These annealed samples were then further used for all the measurement purposes.

2.2. Measurements and Characterizations

The X-ray diffraction (XRD) pattern of the optimized Tm^{3+}/Tm^{3+}-Yb^{3+} doped/codoped $Na_2Y_2B_2O_7$ phosphors have been recorded in the range of 5^0 to 90^0 (2θ degree) by using X-ray diffractrometer. Field emission scanning electron microscopy (FE-SEM) and transmission electron microscopy (TEM) characterizations have been done to have the clear information about the morphology and particle size of the resulting phosphors. The absorption spectra of the prepared phosphors have been recorded in the 300 -1300 nm range. The UC emission studies have been done by using 980nm continuous wave (CW) diode laser excitation source and a monochromator having photomultiplier tube (PMT) attached with a personal computer. Temperature dependent UC emission intensity measurements have been performed with small square shaped homemade furnace and the temperature produced inside the furnace was monitored by holding a copper thermocouple. The temperature of the sample was measured at distance of ~2 mm apart from the laser irradiated focal point. Diode laser focal spot size (area ~1.54 mm^2) and thickness (~0.5 mm) of the samples were kept fixed in all the conditions. All the measurements were performed at ~27^0C temperature.

3. Results and discussion

3.1. XRD study

Fig. 1 shows the XRD pattern of optimized Tm^{3+}/Tm^{3+}-Yb^{3+} doped/codoped $Na_2Y_2B_2O_7$ phosphor. The XRD pattern confirms that the prepared phosphor is of monoclinic phase with space group P121/C and cell parameters, a=10.5969 Å, b=6.2291 Å, c=10.2216 Å; $\alpha = \gamma = 90^0$, $\beta=117.75^0$; V=597.1022 $Å^3$ [11]. From the figure, XRD pattern matches well with the ICSD Collection Code No. 245226 and no any additional peak has been found, which clearly

indicates that the dopants (Tm^{3+} and Tm^{3+}-Yb^{3+}) are successfully introduced in the host lattice [11, 13]. The average crystallite size for doped/codoped $Na_2Y_2B_2O_7$ phosphor has been calculated from the XRD peaks analysis by using well known Debye Scherrer's formula [8]. The average crystallite size for both the phosphors is found around ~18nm and ~20nm respectively.

3.2. FE-SEM and TEM analysis

The FE-SEM characterizations for the developed phosphors have been performed. Fig. 2 shows the FE-SEM micrograph of the optimized Tm^{3+}-Yb^{3+} codoped $Na_2Y_2B_2O_7$ phosphor. The surface morphology of the prepared phosphor tells that the large numbers of small particles are in agglomerated structure having size in nanometre range. The inhomogeneous distribution of the particles is due to the unbalanced flow of temperature and mass in combustion flame during the combustion synthesis process [1]. To get a clear view about the size of the particles, TEM and HRTEM images of the Tm^{3+}-Yb^{3+} codoped $Na_2Y_2B_2O_7$ phosphors have been taken. Fig. 3(a, b) shows the low magnification TEM images with different resolutions. The HRTEM image of the Tm^{3+}-Yb^{3+} codoped $Na_2Y_2B_2O_7$ phosphor is shown in Fig. 3(c). The interplanar spacing has been calculated with the help of sensible lattice fringes observed in the HRTEM image. The interplanar spacing is found to be 0.295 nm, which corresponds to the (120) plane of monoclinic $Na_2Y_2B_2O_7$ nanoparticle (ICSD Collection Code No. 245226). The average size of the particles is observed to be ~20 ± 5 nm which is reasonably in good agreement with the XRD study. Fig. 3(d) represents the electron diffraction pattern of the prepared Tm^{3+}-Yb^{3+} codoped $Na_2Y_2B_2O_7$ phosphor. The detectable circular rings clearly identify the poly-nanocrystalline nature of the prepared phosphor

3.3. Absorption study

The electronic absorption spectra of the Tm^{3+}/Tm^{3+}-Yb^{3+} doped/codoped $Na_2Y_2B_2O_7$ phosphors have been recorded. Four bands around ~460 nm, ~684 nm, ~789 nm and ~1208 nm corresponding to the transitions from the $^3H_6$ (ground state) to different excited states namely $^1G_4$, $^3F_3$, $^3H_4$ and $^3H_5$ for Tm^{3+} doped $Na_2Y_2B_2O_7$ phosphors have been observed in the 300-1300 nm wavelength range, whereas for the Tm^{3+}-Yb^{3+} codoped $Na_2Y_2B_2O_7$ phosphors one extra band around ~980 nm along with all the above said absorption bands have been detected (Fig. 4). In the case of Tm^{3+} singly doped phosphor no absorption at 980 nm is observed. The band around 980 nm is due to the $^2F_{7/2}$←$^2F_{5/2}$ absorption transition of Yb^{3+} ion.

3.4. Upconversion emission study

The UC emission spectra for Tm^{3+}/Tm^{3+}-Yb^{3+} doped/codoped $Na_2Y_2B_2O_7$ phosphors in the range of 400-900 nm range have been recorded by 980 nm CW diode laser excitation. A comparison of UC emission bands for doped/codoped $Na_2Y_2B_2O_7$ phosphor has been shown in Fig. 5. Three leading UC emission bands for the $^1G_4$→$^3H_6$ (488 nm), $^1G_4$→$^3F_4$ (655 nm) and $^3H_4$→$^3H_6$ (814 nm) transitions have been monitored. From this figure, it is clearly observed that the codoping of Yb^{3+} ions enhanced the UC emission intensity significantly. In addition to these UC emission bands some others bands in the Tm^{3+}-Yb^{3+} codoped $Na_2Y_2B_2O_7$ phosphor are also observed around ~264 nm, ~298 nm, and ~362 nm due to the $^3P_2$→$^3H_6$, $^1I_6$→$^3H_6$ and $^1D_2$→$^3H_6$ transitions respectively (Fig. 5). No UC emission band in the UV region was detected for the singly Tm^{3+} doped $Na_2Y_2B_2O_7$ phosphor. The appearance of UC emission bands in the UV region emitted from the higher levels of Tm^{3+} in case of the codoped phosphor is basically due to the strong energy transfer from the Yb^{3+} to Tm^{3+} ions.

For the optimization of dopant ions concentration a series of Tm^{3+}/Tm^{3+}-Yb^{3+} doped/codoped $Na_2Y_2B_2O_7$ phosphors have been prepared by varying the rare earths ions concentration. The

graph of UC emission intensity versus dopants concentration has been shown in Fig. 6. The optimum concentrations for the Tm^{3+} and Tm^{3+}-Yb^{3+} in the doped/codoped $Na_2Y_2B_2O_7$ phosphors are noted to be 0.4 wt% (Tm^{3+}) and 0.4 wt% (Tm^{3+}) – 2 wt% (Yb^{3+}) respectively (Fig. 6). On further increasing the dopants ions concentration above the optimum value, due to the effect of concentration quenching a gradual reduction in the UC emission intensity was observed.

3.5. Energy level diagram, pump power dependence study and colour tunability

In singly Tm^{3+} doped $Na_2Y_2B_2O_7$ phosphor three UC emission bands viz. blue (~488 nm), red (~655 nm) and NIR (~814 nm) have been observed corresponding to the $^1G_4 \rightarrow {}^3H_6$, $^1G_4 \rightarrow {}^3F_4$ and $^3H_4 \rightarrow {}^3H_6$ transitions respectively. The number of NIR photons responsible for these UC emissions can be calculated from the pump power versus UC emission dependence study,

$$I \propto p^n \qquad \text{(i)}$$

where, 'I' is the UC emission intensity, 'p' is the pump power and 'n' is the number of NIR pump photons linked in the UC emission process. From the pump power dependence study the calculated slope values are noted to be 2.76, 2.62 and 1.58 for the UC bands in the blue, red and NIR regions respectively (Fig. 7). In case of the Tm^{3+} doped phosphor, $^3H_4$ and $^1G_4$ level is populated by the involvement of two and three NIR photons respectively [29, 30]. No absorption band around ~980 nm in the Tm^{3+} doped phosphor is detected (Fig. 4). The stepwise non-resonant sequential 980 nm photon absorption in the Tm^{3+} is accountable for these UC emissions [31]. The ground state absorption (GSA) from the $^3H_6$ is non-resonant with the $^3F_4$ level of Tm^{3+} ion; therefore, GSA absorption promotes the ground state population to the $^3F_4$ level non-radiatively (Fig. 9). After that, the $^3F_4$ level population by absorbing 980 nm photon gets lifted into the $^3F_2$ level through first excited state absorption (ESA-1) process. The $^3F_2$ and $^3F_3$ levels are very close and therefore treated as thermally

coupled levels. The population of $^3F_2$ (~14975 cm^{-1}) level relaxes non-radiatively to the $^3H_4$ (~12517 cm^{-1}) level via the emission of five number of phonons. The $^3H_4$ level is again partially depopulated radiatively and emits a NIR photon through the $^3H_4 \rightarrow {}^3H_6$ transition. The rest part of population accumulated in the $^3H_4$ level helps in populating the $^1G_4$ level via the second excited state absorption (ESA-2) process. The population of $^1G_4$ level decays radiatively to the $^3H_6$ and $^3F_4$ levels and emits two radiative photons in the blue and red regions corresponding to the $^1G_4 \rightarrow {}^3H_6$ and $^1G_4 \rightarrow {}^3F_4$ transitions respectively. The blue/red and blue/NIR emission intensity ratio is found to be 6.93 and 0.29 respectively in the singly Tm^{3+} doped phosphor.

For Tm^{3+}-Yb^{3+} codoped $Na_2Y_2B_2O_7$ phosphor in addition to the aforementioned emission bands three more UC emission bands have been observed under the 980 nm diode laser excitation. These additional UC emission bands are observed at ~264 nm, ~298 nm, ~362 nm corresponding to the $^3P_2 \rightarrow {}^3H_6$, $^1I_6 \rightarrow {}^3H_6$ and $^1D_2 \rightarrow {}^3H_6$ transition respectively. Energy level diagram with their UC mechanisms for the Tm^{3+}-Yb^{3+} codoped $Na_2Y_2B_2O_7$ phosphor irradiated by 980 nm CW diode laser source has been depicted in Fig. 9. In order to discuss the involved processes responsible for the observed UC emissions, pump power dependence study has been performed (Fig. 8).

From Fig. 8, the slope values for, ~264 nm, ~362 nm, ~488 nm, ~655 nm and ~814 nm transitions are 3.80, 2.62, 2.48, 1.84 and 1.54 respectively. Since the absorption cross-section of Yb^{3+} ion is large and hence it absorbs the pump photons efficiently when excited with a less expensive 980nm laser diode [15]. As in the codoped samples a broad band around ~980 nm corresponding to the Yb^{3+} ion is observed (Fig. 4), therefore the NIR photons are efficiently absorbed by the Yb^{3+} ions. In the Tm^{3+}-Yb^{3+} codoped system the concentration of Yb^{3+} is generally high; therefore the UC mechanism is mainly due to strong energy transfer (ET) from Yb^{3+} to Tm^{3+} ions [32]. The excited Yb^{3+} ions after absorbing 980 nm photon,

transfer its excitation energy to the Tm^{3+} ions by the ET-1 process non-resonantly. The ground state Tm^{3+} ions after getting the energy from the Yb^{3+} ions by the ET-1 process gets excited to the $^3H_5$ level (~8229 cm^{-1}) by the emission of four numbers of phonons [33]. The $^3H_5$ level is depopulated through nonradiative relaxations into the $^3F_4$ level (~5545 cm^{-1}) by multiphonon emission process. The population of $^3F_4$ level is again promoted via ET-2 process into the $^3F_2$ level. The $^3F_2$ (~14975 cm^{-1}) level is depopulated to the $^3H_4$ (~12517 cm^{-1}) level by the emission of five number of phonons [33]. A part of the population of the $^3H_4$ level is transferred to the $^1G_4$ level via ET-3 process and the remaining population via the radiative relaxation to the ground state emits a photon at ~814 nm corresponding to the $^3H_4 \rightarrow {}^3H_6$ transition. The population available in the $^1G_4$ level relaxes to the $^3H_6$ and $^3F_4$ level through the radiative transitions and emit photons in the blue and red regions respectively. From the pump power study the slope values for UC bands at ~488 nm and ~362 nm are noted to be ~2.48 and ~2.62 respectively. The decrease in the slope values is due to the effect of energy transfer and cooperative sensitization which causes an increase in the energy transfer rate from Yb^{3+} to Tm^{3+} ions [20, 34-37]. In the codoped phosphor blue UC emission intensity is large e``nough compared to the other emissions. The intensity enhancement due to codoping with Yb^{3+} ions about ~1000, ~160 and ~98 times for blue, red and NIR bands respectively have been resulted. Moreover, the blue/red and blue/NIR emission intensity ratio in codoped phosphor is improved from 6.93 to 42.90 and 0.29 to 3.0 respectively. This giant enhancement for the UC emission intensity in the codoped phosphor makes it superior from the other reported materials [30, 38-41]. Thus the energy transfer and the feasible cooperative sensitization processes are responsible for such an enormous enhancement. Moreover, the cooperative sensitization and cross-relaxation (CR-1) process ($^3H_5 + {}^1G_4 \rightarrow {}^3H_6 + {}^1D_2$) helps in populating the $^1D_2$ level. The energy mismatch during the cross-relaxation process is compensated by the emission of three number of phonons. The A part of the $^1D_2$ level

population appears to be promoted to the $^3P_2$ level by the ET-4 process [35]. The rest of the population stored in the $^1D_2$ level is depopulated by the emission of a photon peaking at ~362 nm through the $^1D_2 \rightarrow {}^3H_6$ transition [36]. As the slope value for ~264 nm UC emission band is 3.80 which imply that four number of 980 nm photons are responsible for populating the $^3P_2$ level (Fig. 8). The $^3P_2$ level may also be populated through the cross-relaxation (CR-2) process ($^1G_4 + {}^3F_2 \rightarrow {}^3H_6 + {}^3P_2$). The $^3P_2$ level is depopulated in two steps, in the first step one part of the population is utilized in the radiative emission at ~264 nm through the $^3P_2 \rightarrow {}^3H_6$ transition and in the second step the rest of the population relaxes nonradiatively to the $^1I_6$ level through the multiphonon emissions [35, 36]. The radiative transition corresponding to the $^1I_6 \rightarrow {}^3H_6$ transition emits a photon at ~298nm [36]. The decay curve analysis for the blue emitting level ($^1G_4$) has been performed (Fig. 10). The observed decay (τ) time is found to be ~685 ± 0.1 μs and ~432 ± 0.7 μs for doped and codoped phosphor, respectively. The observed decay time in the case of codoped phosphor is shorter than the singly Tm^{3+} doped phosphor which also proves the effect of efficient energy transfer from Yb^{3+} to Tm^{3+} ion [1, 31]. It is well known that the radiative transition probability follows an inverse law with decay time of the emitting level [42, 43]. In the present case it is observed that the decay time corresponding to blue light emitting level has been reduced due to addition of Yb^{3+} ion and hence the radiative transition probability is increased [1]. This result further support the existence of energy transfer mechanism in the codoped phosphor.

For Tm^{3+}-Yb^{3+} codoped $Na_2Y_2B_2O_7$ phosphor the colour coordinates at different pump power densities have been calculated by using the GoCIE software. The colour coordinates do not vary with the pump power density and the all colour coordinates lye in the blue region of the chromaticity diagram. The small deviation in the colour coordinates may be due to the fluctuations in the pump power at different scans (Table. 2). The average value of the colour coordinate (X=0.09, Y=0.17) is found to be within the blue region. Thus the prepared

material emits efficient blue colour which is not tunable even at higher excitation densities from 1.36 to 66.88 W/cm^2 and hence may be useful for making the efficient blue upconverter and display devices.

3.6. Optical temperature sensing study

The UC emission spectra of the codoped nanophosphor at different temperatures have been recorded. Fig. 11 shows the UC emission spectra in the wavelength range from 440-520 nm at measured temperatures of 300 K, 443 K and 623 K for Tm^{3+}-Yb^{3+} codoped $Na_2Y_2B_2O_7$ phosphor. The pump power density of 980 nm CW laser diode has been fixed at 34.87 W/cm^2. Two distinct blue UC emission peaks centred at 477 and 488 nm corresponding to the $^1G_4 \rightarrow {}^3H_6$ transition of Tm^{3+} ions have been observed [20]. These two peaks are due to the transitions from the stark sublevels of the $^1G_4$ level to $^3H_6$ level. On varying the temperature range from 300 to 623 K, no change in the peak positions has been noted but the intensity ratio know as 'fluorescence intensity ratio (FIR)' of two thermally coupled sublevels are altered significantly. Due to the thermal effect the intensity of the whole band lying in the blue region is reduced very much but the variations in the intensity of these two peaks (stark components) is different. The intensity of the peak at ~ 477 nm increases gradually with increasing the temperature whereas the intensity of the peak at ~ 488 nm decreases. Pérez-Rodríguez et al. [44] reported, that there is a high probability of non-radiative relaxations between the two sublevels that keeps them thermally coupled (i.e. each level is optically coupled to a lower common level). Due to the small energy gap (~ 473 cm^{-1}) between two thermally coupled $^1G_{4(i)}$ and $^1G_{4(j)}$ sublevels of the $^1G_4$ level, these sublevels are considered as in quasi-thermal equilibrium with each other [20, 24]. Therefore, the population of these sublevels follow Boltzmann-type population distribution [24, 45]. As the UC emission

intensity ratio corresponding to the $^1G_{4(j)} \rightarrow {}^3H_6$ and $^1G_{4(i)} \rightarrow {}^3H_6$ transitions vary with change in temperature. Therefore the intensity ratio can be described by the following expression [46],

$$\text{FIR} = \frac{I_{477}}{I_{488}} = R \exp(-\Delta E / kT) \qquad \text{(ii)}$$

where, I_{477} and I_{488} is the integrated intensity of the stark components peaking at 477 nm and 488nm respectively, R is the proportionality constant, ΔE is the energy gap between the two stark sublevels, k and T is the Boltzmann's constant and absolute temperature respectively.

The integrated intensity for both I_{477} and I_{488} of the UC emission bands have been taken for the calculation of the intensity ratio (I_{477}/I_{488}). A logarithmic plot for I_{477}/I_{488} versus inverse of temperature is given in Fig. 12. It has been observed that the FIR changes slowly from 0.64 to 1.84 as the temperature increases from 300 to 623K. The equation (ii) has been fitted well with the experimentally observed values. By using the slope calculated from the Fig. 12, the energy gap between the two stark sublevels has been determined. From the estimated slope value, the energy gap 'ΔE' is ~445.80 cm^{-1}. The observed energy gap between these two sublevels is ~473 cm^{-1} and is in close agreement with the experimentally determined energy gap (~445.80 cm^{-1}).

The sensor sensitivity is an important parameter for the development of highly sensitive optical temperature sensor. The change in FIR for thermally coupled sublevels with temperature results the sensitivity, the sensitivity of the Tm^{3+}-Yb^{3+} codoped $Na_2Y_2B_2O_7$ phosphor has been calculate by using the following relation [23],

$$S = \frac{d(FIR)}{dT} = \text{FIR}\ (\Delta E \setminus kT^2) \qquad \text{(iii)}$$

In the dual-Y axis plot of Fig. 13, calculated sensitivity of Tm^{3+}-Yb^{3+} codoped $Na_2Y_2B_2O_7$ phosphor with the variation of temperature has been plotted. The maximum sensitivity of

Tm^{3+}-Yb^{3+} codoped $Na_2Y_2B_2O_7$ phosphor is 4.54×10^{-3} K^{-1} at 300K and seems to increase in the low temperature region. The minimum sensitivity ~3.03×10^{-3} K^{-1} within 300-623 K temperature range is observed at 623 K. On further increasing the temperature, the fluorescence intensity arising from these thermally coupled sublevels are diminished very much therefore the measurement of FIR becomes unfeasible. Moreover, we have compared our results with the other reported similar works based on sensitivity of two coupled levels (Table. 1). Table. 1 contains sensor sensitivity at particular temperature of different RE ions doped sensing materials with their optical transitions. From the Table. 1, it is concluded that the sensor sensitivity of Tm^{3+}-Yb^{3+} codoped $Na_2Y_2B_2O_7$ phosphor is significant for temperature sensing measurement in the range of 300-623 K. The above demonstration supports that the Tm^{3+}-Yb^{3+} codoped $Na_2Y_2B_2O_7$ phosphor is suitable for the temperature sensor and thermometry measurement within the 300-623 K temperature range with high sensitivity.

3.7. Optical nanoheater based study

In order to monitor the internal heating produced in the codoped phosphor at a particular laser excitation power density, we have calculated the FIR at different pump power densities from 1.36 to 66.88 W/cm^2 for the blue UC emissions at 477 nm and 488 nm. A plot of FIR (i.e. I_{477}/I_{488}) versus pump power density at room temperature is shown in Fig. 14. The value of FIR appears to increase from 0.44 to 0.96 with increasing the pump power density from 1.36-66.88 W/cm^2. Variation in FIR with the pump power density permits the study of temperature rising in the developed sample and hence leads to the thought of nano-volume based optical nanoheater [2, 47]. Equation (ii) can be subsequently changed into an easy form given below.

$$\ln\frac{I_{477}}{I_{488}} = \ln R - \Delta E / kT \qquad \text{(iv)}$$

where, all the terms have their usual meanings. This equation indicates that FIR is apparently related to the temperature 'T' of the emitting sample. The value of constant 'R' and 'ΔE' is experimentally determined by using the temperature dependent UC emission study of the prepared sample (Fig. 12 and Fig. 13). By using equation (iv), temperature gain has been calculated at different pump power densities and plotted in the right side of Y-axis dual plot (Fig. 14). At maximum laser power density 66.88 W/cm^2 a temperature rise of about 440 K has been observed for the Tm^{3+}-Yb^{3+} codoped $Na_2Y_2B_2O_7$ phosphor. In order to verify the temperature rise we have placed the values of FIR obtained at that particular pump power density in the temperature dependence FIR variations (shown in the Fig. 13). The temperature gain of about 435 K for FIR ~0.96 corresponding to the pump power density of 66.88 W/cm^2 is marked. This value (~435 K) is reliable and is in close agreement with the temperature gain (440 K) calculated by using the equation (iv).

The nanocrystalline nature of the prepared Tm^{3+}-Yb^{3+} codoped $Na_2Y_2B_2O_7$ phosphor can efficiently generate the heat by 980 nm diode laser excitation. By the optical excitation large number of mobile charge carriers may interact through the electric field of the radiation used for the excitation inside the nano-crystalline phosphor. Therefore, the energy gaining electrons are capable to renovate the excitation energy into heat via nonradiative channels or electron-phonon coupling [21, 26]. Verma et al. have reported that heat developed from the nano-crystalline phosphor turns to increase the temperature of the surrounding volume [21]. The quantum confinement of phonons in the nano-crystalline phosphor cannot be neglected, as it promotes the electron-phonon coupling [2, 26], which is beyond the scope of present investigation. Therefore, the prepared Tm^{3+}-Yb^{3+} codoped nanophosphor also plays a dominant role for converting the absorbed energy into the thermal energy around the surrounding environment due to their large surface/volume ratio [21].

Recently, hyperthermia has been helpful as a heating therapy with a variety of cancer treatments such as radiotherapy, chemotherapy, drug delivery and other radiation treatments. For hyperthermia treatment the temperature requirement is in the range of 314-318 K, which is useful for heating the affected cells or tissues and has a direct cell-killing effect, specifically in defective parts of the tumour. The developed phosphor is competent to produce hyperthermia treatment temperature at low pump power density ~7.0 W/cm^2 upon excitation at 980 nm radiation (Fig. 13).

4. Conclusion

The efficient blue frequency upconversion upon excitation at 980nm in the monoclinic phase Tm^{3+}-Yb^{3+} codoped $Na_2Y_2B_2O_7$ nanophosphor synthesized successfully by solution combustion method and characterized by XRD, FE-SEM, TEM and absorption study techniques have been reported. The maximum enhancement about ~1000 times in the blue UC emission band on codoping with Yb^{3+} ions has been observed and explained due to the energy transfer and cooperative sensitization processes. The maximum sensor sensitivity ~4.54×10^{-3} K^{-1} has been determined at room temperature and appears to increase in the lower temperature region. The laser induced optical heating behaviour has been performed by considering the FIR variation as a function of pump power density. The maximum temperature gain of about ~435 K calculated at 66.88 W/cm^2 laser power density has been detected. The NIR laser induced study suggests that the developed nanophosphor may be of significant interest in hyperthermia based treatment. The colour coordinates at different pump power densities have been calculated and no significant deviation has been reported. On the basis of the observed experimental data, the developed nanophosphor can be used as multifunctional material for a variety of applications viz. NIR to blue upconverter, temperature sensor, medical diagnosis and blue display devices.

Acknowledgements

Authors acknowledge the financial support from University Grant Commission (UGC), New Delhi, India. Mr. Abhishek Kumar Soni is also very much thankful to Indian School of Mines, Dhanbad, India for providing the financial assistance.

References

[1] Pandey, A.; Rai, V. K.; Improved Luminescence and Temperature Sensing Performance of Ho^{3+}–Yb^{3+}–Zn^{2+}:Y_2O_3 Phosphor Dalton Trans. **2013**, 4, 11005-11011.

[2] Singh, S. K.; Kumar, K.; Rai, S. B.; Diode Laser Pumped Gd_2O_3:Er^{3+}/Yb^{3+} Phosphor as Optical Nano-Heater Appl. Phys. B. **2010**, 100, 443-446.

[3] Richards, B. S.; Enhancing the Performance of Silicon Solar Cells via the Application of Passive Luminescence Conversion Layers Sol. Energ. Mat. Sol. C. **2006**, 90, 2329-2337.

[4] Cao, T.; Yang, Y.; Gao, Y.; Zhou, J.; Li, Z.; Li, F.; High-Quality Water-Soluble and Surface-Functionalized Upconversion Nanocrystals as Luminescent Probes for Bioimaging Biomaterials. **2011**, 32, 2959-2968.

[5] Liu, L.; Zhang, Z.; Zhang, L.; Zhai, Y.; The Effectiveness of Strong Afterglow Phosphor Powder in the Detection of Finger Marks Forensic Sci. Int. **2009**, 183, 45-49.

[6] Atabaev, T.; Hwang, Y-H.; Kim, H-K.; Color-Tunable Properties of Eu^{3+}- and Dy^{3+}-Codoped Y_2O_3 Phosphor Particles Nanoscale Res. Lett. **2012**, 7, 556-562.

[7] Saito, M.; Nakamura, S.; Kita, T.; Fast-Response Signal Upconversion by the Use of a "Time-Space Conversion" Method Appl. Phys. Lett. **2011**, 99, 191101-191104.

[8] Lei, F.; Yan, B.; Hydrothermal Synthesis and Luminescence of $CaMO_4:RE^{3+}$ (M=W, Mo; RE=Eu, Tb) Submicro-Phosphors J. Solid State Chem. **2008,** 181, 855-862.

[9] Guo, C.; Yu, J.; Jeong, J-H.; Ren, Z.; Bai, J.; Effect of Eu^{3+}Contents on the Structure and Properties of $BaLa_2ZnO_5:Eu^{3+}$ Phosphors Physica B **2011**, 406, 916-920.

[10] Havlak, L.; Jary, V.; Nikl, M.; Bohacek , P.; Barta, J.; Preparation, Luminescence and Structural Properties of RE-Doped $RbLaS_2$ Compounds Acta Mater. **2011,** 59, 6219-6227.

[11] Wen, D.; Shi, J.; A Novel Narrow-Line Red Emitting $Na_2Y_2B_2O_7:Ce^{3+},Tb^{3+},Eu^{3+}$ Phosphor with High Efficiency Activated by Terbium Chain for Near-UV White LEDs Dalton Trans. **2013**, 42, 16621-16629.

[12] Quintanilla, M.; Cantelar, E.; Cusso´, F.; Villegas, M.; Caballero, A. C.; Temperature Sensing with Up-Converting Submicron-Sized $LiNbO_3:Er^{3+}/Yb^{3+}$ Particles Appl. Phys. Express, **2011**, 4, 022601-022604.

[13] Wen, D.; Yang, H.; Yang, G.; Shi, J.; Wu, M.; Su, Q.; Structure and Photoluminescence Properties of $Na_2Y_2B_2O_7:Ce^{3+},Tb^{3+}$ Phosphors for Solid-State Lighting Application J. Solid State Chem. **2014**, 213, 65-71.

[14] Koparkar, K. A.; Bajaj, N. S.; Omanwar, S. K.; A Potential Candidate for Lamp Phosphor: Eu^{3+} Activated $K_2Y_2B_2O_7$ Adv. Opti. Techn. **2014**, 5, 706459-706463.

[15] Milanese, D.; Gebavi, H.; Lousteau, J.; Ferraris, M.; Schulzgen, A.; Li, L.; Peyghambarian, N.; Taccheo, S.; Auzel, F.; $Tm^{3+}$and Yb^{3+} Co-doped Tellurite Glasses for Short Cavity Optical Fiber Lasers: Fabrication and Optical Characterization J. Non-Cryst. Solids. **2010**, 356, 2378-2383.

[16] Das, S.; Reddy, A. A.; Vijaya Prakash, G.; Strong Green Upconversion Emission from Er^{3+}–Yb^{3+} Co-doped $KCaBO_3$ Phosphor Chem. Phys. Lett. **2011**, 504, 206-210.

[17] Ostermayer, F. W.; Jr; vander Ziel, J. P.; Marcos, H. M.; Van Uitert, L. G.; Geusic, J. E.; Frequency Upconversion inYF_3:Yb^{3+}, Tm^{3+} Phys. Rev. B **1971,** 3, 2698-2705.

[18] Collins, S. F.; Baxter, G. W.; Wade, S. A.; Sun, T.; Grattan, K. T. V.; Zhang, Z. Y.; Palmer, A. W.; Comparison of Fluorescence-Based Temperature Sensor Schemes: Theoretical Analysis and Experimental Validation J. Appl. Phys. **1998,** 84, 4649-4654.

[19] Rai, V. K.; Temperature Sensors and Optical Sensors Appl. Phys. B. **2007**, 88, 297-303.

[20] Li, D.; Wang, Y.; Zhang, X.; Yang, K.; Liu, L.; Song Y.; Optical Temperature Sensor Through Infrared Excited Blue Upconversion Emission in $Tm^{3+/}Yb^{3+}$ Codoped Y_2O_3 Opt. Commun. **2012**, 285, 1925-1928.

[21] Verma, R. K.; Rai, S. B.; Laser Induced Optical Heating From Yb^{3+}/Ho^{3+}: $Ca_{12}Al_{14}O_{33}$ and Its Applicability as a Thermal Probe J. Quant. Spectrosc. Ra. **2012**, 113, 1594-1600.

[22] Rai, V. K.; Rai, S. B.; Temperature Sensing Behaviour of the Stark Sublevels Spectrochim. Acta Part A. **2007,** 68, 1406-1409.

[23] Xu, W.; Gao, X.; Zheng, L.; Wang, P.; Zhang, Z.; Cao, W.; Optical Thermometry Through Green Upconversion Emissions in Er^{3+}/Yb^{3+}-Codoped $CaWO_4$ Phosphor Appl. Phys. Express. **2012**, 5, 072201-072203.

[24] Joshi, C.; Dwivedi, A.; Rai, S. B.; Structural Morphology, Upconversion Luminescence and Optical Thermometric Sensing Behavior of $Y_2O_3:Er^{3+}/Yb^{3+}$ Nano-Crystalline Phosphor Spectrochim. Acta Part A. **2014**, 129, 451-456.

[25] Singh, S. K.; Kumar, K.; Rai, S. B.; Diode Laser Pumped $Gd_2O_3:Er^{3+}/Yb^{3+}$ Phosphor as Optical Nano-Heater Appl. Phys. B. **2010**, 100, 443-446.

[26] Dey, R.; Pandey, A.; Rai, V. K.; Er^{3+}-Yb^{3+} and Eu^{3+}-Er^{3+}-Yb^3 Codoped Y_2O_3 Phosphors as Optical Heater Sens. Actuators B. **2014**, 190, 512-515.

[27] Van der Zee, J.; Heating the Patient: A Promising Approach? Ann. Oncol. **2002**, 13 (8) 1173-1184.

[28] Chatterjee, D. K.; Rufaihah, A. J.; Zhang, Y.; Upconversion Fluorescence Imaging of Cells and Small Animals Using Lanthanide Doped Nanocrystals Biomaterials. **2008**, 29, 937-943.

[29] Li, L.; Xiaochun, W.; Xiantao, W.; Yonghu, C.; Changxin, G.; Min, Y.; Influence of Precipitant Solution pH On the Structural, Morphological and Upconversion Luminescent Properties of Lu_2O_3:2%Yb, 0.2%Tm Nanopowders Physica B. **2011**, 406 609-613.

[30] Mohanty, D. K.; Rai, V. K.; Dwivedi, Y.; Yb^{3+} Sensitized Tm^{3+} Upconversion in Tellurite Lead Oxide Glass Spectrochim. Acta Part A, **2012**, 89, 264-267.

[31] Soni, A. K.; Rai, V. K.; Intrinsic Optical Bistability and Frequency Upconversion in Tm^{3+}-Yb^{3+} Codoped Y_2WO_6 Phosphor Dalton Trans., **2014**, 43, 13563-13570.

[32] Borja-Urby, R.; Diaz-Torres, L. A.; Salas, P.; Vega-Gonzalez, M.; Angeles-Chavez, C.; Blue and Red Emission in Wide Band Gap $BaZrO_3$:Yb^{3+}, Tm^{3+} Mater. Sci. Eng. B. **2010**, 174, 169-173.

[33] Dieke, G. H.; Spectra and Energy Levels of Rare Earth Ions in Crystals, Interscience Publishers, USA, **1968**, pp. 310-313 [ISBN 470 213906].

[34] Kumari, A.; Rai, V. K.; Kumar, K.; Yellow–Orange Upconversion Emission in Eu^{3+}–Yb^{3+} Codoped $BaTiO_3$ Phosphor Spectrochim. Acta, part A. **2014**, 127, 98-101.

[35] Cao, B. S.; Wu, J. L.; Feng, Z. Q.; Dong, B.; Investigation of Near-Infrared-to-Ultraviolet Upconversion Luminescence of Tm^{3+} Doped $NaYF_4$ Phosphors by Yb^{3+} Codoping Mater. Chem. Phys., **2013**, 142, 333-338.

[36] Zhang, D.; Qin, W.; Wang, G.; Wei, G.; Wang, L.; Zhu, P.; Kim, R.; Ding, F.; Zheng, K.; Liu, N.; Synthesis and Upconversion Luminescence of YF_3:Yb^{3+} Tm^{3+} and TiO_2-Coated YF_3:Yb^{3+}, Tm^{3+} Microcrystals J. Nanosci. Nanotechnol. **2010**, 10, 2032-2036.

[37] Wang, G.; Qin, W.; Wang, L.; Wei, G.; Zhu, P.; Kim, R.; Intense Ultraviolet Upconversion Luminescence From Hexagonal $NaYF_4$:Yb^{3+}/Tm^{3+} Microcrystals Opt. Express. **2008**, 16, 11907-11914.

[38] de Assumpção, T. A. A.; Kassab, L. R. P.; Gomes, A. S. L.; de Araújo, C. B.; Wetter, N. U.; Influence of the Heat Treatment on the Nucleation of Silver Nanoparticles in Tm^{3+} doped PbO-GeO_2 Glasses Appl. Phys. B. **2011**, 103 165-169.

[39] Mishra, K.; Giri, N. K.; Rai, S.B.; Preparation and Characterization of Upconversion Luminescent Tm^{3+}/Yb^{3+} Co-doped Y_2O_3 Nanophosphor Appl. Phys. B. **2011**,103, 863-875.

[40] Zhao, C.; Kong, X.; Liu, X.; Tu, L.; Wu, F.; Zhang, Y.; Liu, K.; Zeng, Q.; Zhang, H.; Li^{+} ion Doping: An Approach for Improving the Crystallinity and Upconversion Emissions of $NaYF_4:Yb^{3+}$, Tm^{3+} Nanoparticles Nanoscale. **2013**, 5, 8084-8089.

[41] Sing, B. P.; Parchur, A. K.; Ningthoujam, R. S.; Ramakrishna, P. V.; Singh, S.; Singh, P.; Rai, S. B.; Maalej, R.; Enhanced Up-conversion and Temperature- Sensing Behaviour of Er^{3+} and Yb^{3+} Codoped $Y_2Ti_2O_7$ by Incorporation of Li^{+} Ions Phys. Chem. Chem. Phys. **2014**, 16, 22665-22676.

[42] Mohanty, D. K.; Rai, V. K.; Photoluminescence Studies of Pr^{3+} Doped Lead Germanate Glass J. Fluores., **2011**, 21, 1455-1460.

[43] Zou, K.; Guo, H.; Lu, M.; Li, W.; Hou, C.; Wei, W.; He, J.; Peng, B.; Xiangli, B.; Broad-spectrum and long-lifetime emissions of Nd^{3+} ions in lead fluorosilicate glass Opt. Express., **2009**, 17, 10001-10009.

[44] Pérez-Rodríguez, C.; Martín, L. L.; León-Luis, S. F.; Martín, I. R.; Kiran Kumar, K.; Jayasankar, C. K.; Relevance of Radiative Transfer Processes on Nd^{3+} Doped Phosphate Glasses for Temperature Sensing by Means of the Fluorescence Intensity ratio Technique Sens. Actuators B. **2014**, 195, 324-331.

[45] Zhou, S.; Deng, K.; Wai, X.; Jiang, G.; Duan, C.; Chen, Y.; Yin, M.; Upconversion Luminescence of $NaYF_4:Yb^{3+}$, Er^{3+} for Temperature Sensing Opti. Commun. **2013**, 291, 138-142.

[46] Cao, B. S.; He, Y. Y.; Feng, Z. Q.; Li, Y. S.; Dong, B.; Optical Temperature Sensing Behaviour of Enhanced Green Upconversion Emissions From Er–Mo:$Yb_2Ti_2O_7$ Nanophosphor Sens. Actuators B, **2011**, 159, 8-11.

[47] Gluchowski, P.; Strek, W.; Studies of Upconversion Emission of Yb^{3+}, Er^{3+}:Lu_2O_3 Nanoceramics Opt. Mater. **2013**, 35, 731-734.

[48] Wang, X.; Liu , Chun-sheng.; Yan, X.; Optical Temperature Sensing of Hexagonal $Na_{0.82}Ca_{0.08}Er_{0.16}Y_{0.853}F_4$ Phosphor RSC Adv. **2014**, 4, 24170-24175.

[49] Haro-González, P.; Martín, I. R.; Martín, L. L.; León-Luis, S. F.; Pérez-Rodríguez, C.; Lavín, V.; Characterization of Er^{3+} and Nd^{3+} Doped Strontium Barium Niobate Glass Ceramic as Temperature Sensors Opt. Mater. **2011**, 33, 742-745.

[50] Singh, S. K.; Kumar, K.; Rai, S. B.; Er^{3+}/Yb^{3+} Codoped Gd_2O_3 Nano-Phosphor for Optical Thermometry Sens. Actuators A. **2009**, 149, 16-20.

[51] Dong, B.; Cao, B. S.; Feng, Z. Q.; Wang, X. J.; Optical Temperature Sensing Through Extraordinary Enhancement of Green Up-conversion Emissions For Er –Yb–Mo:Al_2O_3 Sens. Actuators B. **2012**, 165, 34-37.

[52] Rakov, N.; Maciel, G. S.; Three-Photon Upconversion and Optical Thermometry Characterization of Er^{3+}:Yb^{3+} Co-doped Yttrium Silicate Powders Sens. Actuators B. **2012**, 164, 96-100.

Table Caption

Table 1: Comparative list for FIR based temperature sensitivity reported by different researchers.

RE doped Sensing Material	*Transitions*	*Range of Temperature*	*Maximum Sensitivity*	*Reference*
$Yb_2Ti_2O_7$ codoped Er^{3+}–Mo	$^2H_{11/2}$, $^4S_{3/2}\rightarrow{}^4I_{15/2}$	290-610K	$7.40\times10^{-3}K^{-1}$ at 290K	[46]
Y_2SiO_5 codoped Er^{3+}-Yb^{3+}	$^2H_{11/2}$, $^4S_{3/2}\rightarrow{}^4I_{15/2}$	300-600K	$5.60\times10^{-3}K^{-1}$ at 375K	[52]
Al_2O_3 codoped Er^{3+}–Yb^{3+}-Mo	$^2H_{11/2}$, $^4S_{3/2}\rightarrow{}^4I_{15/2}$	294-973K	$5.10\times10^{-3}K^{-1}$ at 294K	[51]
$Na_2Y_2B_2O_7$ doped Tm^{3+}-Yb^{3+}	$^1G_{4(i)}$,$^1G_{4(j)}\rightarrow{}^3H_6$	300-623K	$4.54\times10^{-3}K^{-1}$ at 300K	[Present work]
Gd_2O_3 codoped Er^{3+}-Yb^{3+}	$^2H_{11/2}$, $^4S_{3/2}\rightarrow{}^4I_{15/2}$	300-900K	$3.90\times10^{-3}K^{-1}$ at 300K	[50]
Y_2O_3 codoped Tm^{3+}-Yb^{3+}	$^1G_{4(a)}$,$^1G_{4(b)}\rightarrow{}^3H_6$	303-753K	$3.50\times10^{-3}K^{-1}$ at 303K	[20]
Y_2O_3 codoped Ho^{3+}–Yb^{3+}–Zn^{2+}	$^3K_8$, $^5F_3\rightarrow{}^5I_8$	300-673K	$3.01\times10^{-3}K^{-1}$ at 673K	[1]
$Na_{0.82}Ca_{0.08}Er_{0.16}Y_{0.853}F_4$ doped Er^{3+}	$^2H_{11/2}$, $^4S_{3/2}\rightarrow{}^4I_{15/2}$	5-300K	$2.20\times10^{-3}K^{-1}$ at 338K	[48]
Strontium Barium Niobate (SBN) glass ceramic doped Nd^{3+}	$^4F_{5/2}$, $^4F_{3/2}\rightarrow{}^4I_{9/2}$	300-700K	$1.50\times10^{-3}K^{-1}$at 600K	[49]

Table 2: Calculated colour coordinate at different excitation power density excited by 980nm diode laser.

Excitation power density	Colour coordinate values (X, Y)
1.36 W/cm^2	(0.09, 0.16)
7.01 W/cm^2	(0.09, 0.20)
18.50 W/cm^2	(0.09, 0.20)
23.63 W/cm^2	(0.09, 0.18)
29.41 W/cm^2	(0.09, 0.18)
40.12 W/cm^2	(0.10, 0.17)
45.06 W/cm^2	(0.10, 0.17)
50.45 W/cm^2	(0.10, 0.16)
55.84 W/cm^2	(0.10, 0.16)
66.88 W/cm^2	(0.10, 0.16)

Figure Caption

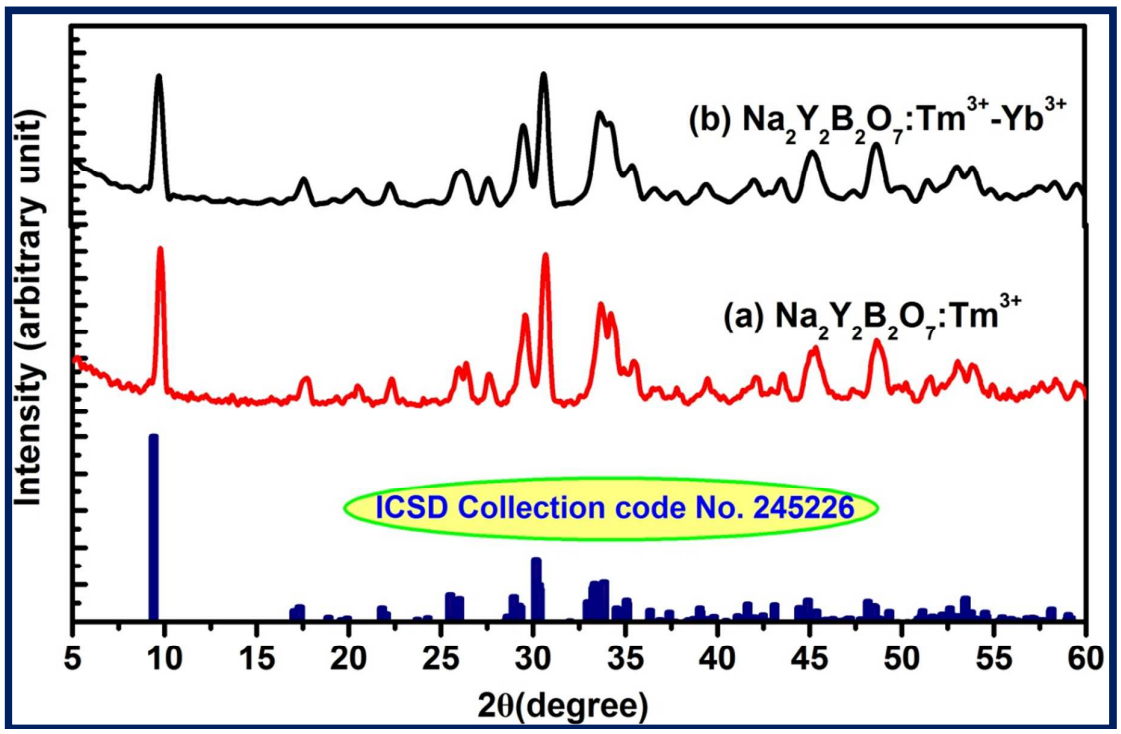

Fig. 1: XRD pattern of Tm^{3+} / Tm^{3+}-Yb^{3+} doped / codoped $Na_2Y_2B_2O_7$ phosphor

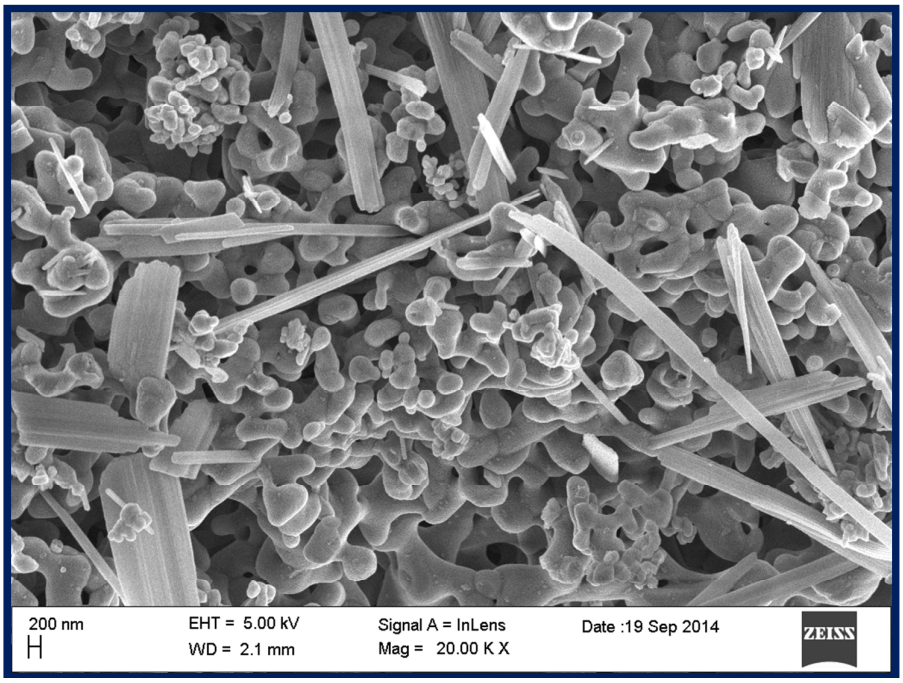

Fig. 2: FE-SEM micrograph of the Tm^{3+}-Yb^{3+} codoped $Na_2Y_2B_2O_7$ phosphor.

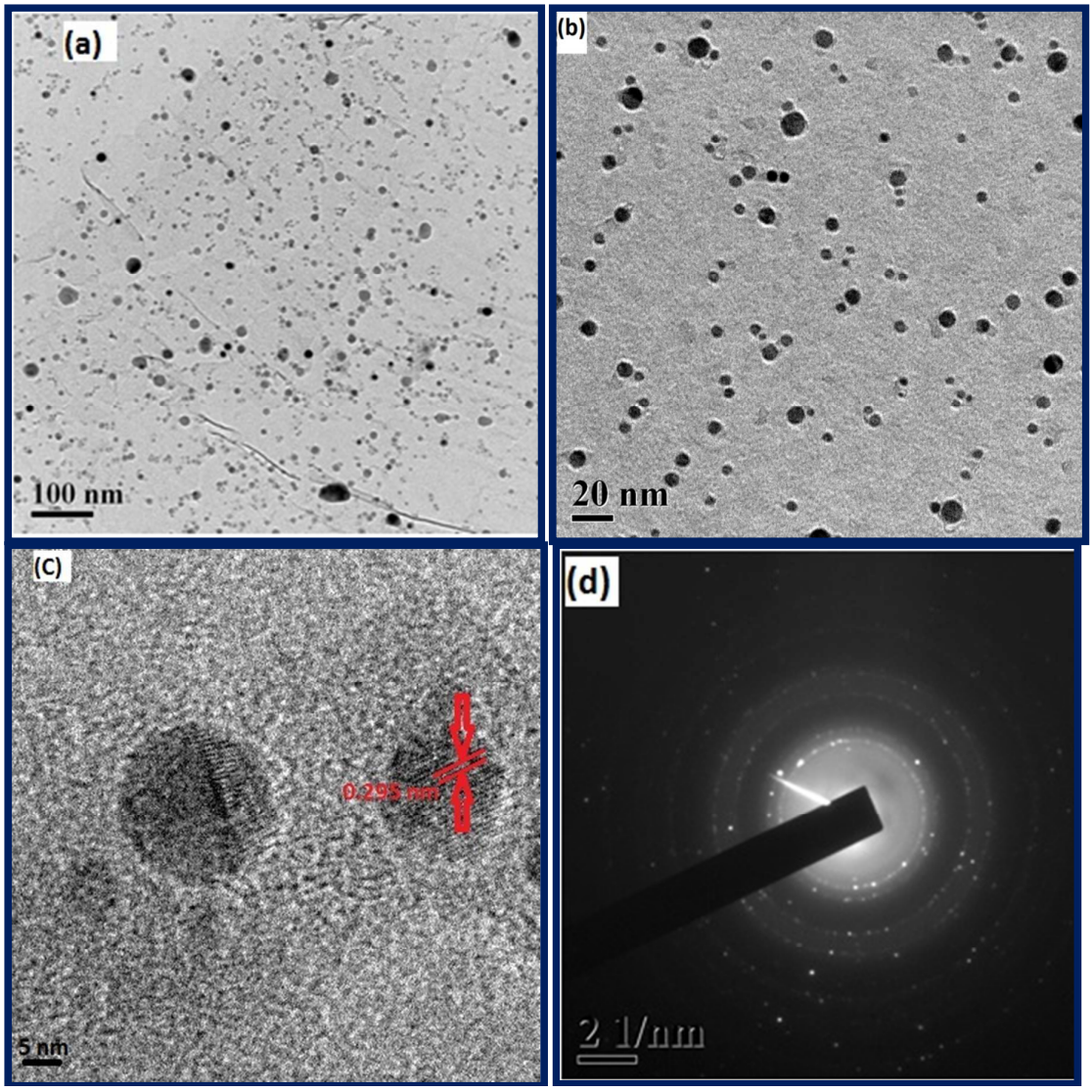

Fig. 3: Transmission electron microscopy images (a) 100nm resolution (b) 20nm resolution (c) high resolution transmission electron microscopy image and (d) electron diffraction pattern of the Tm^{3+}-Yb^{3+} codoped $Na_2Y_2B_2O_7$ phosphor.

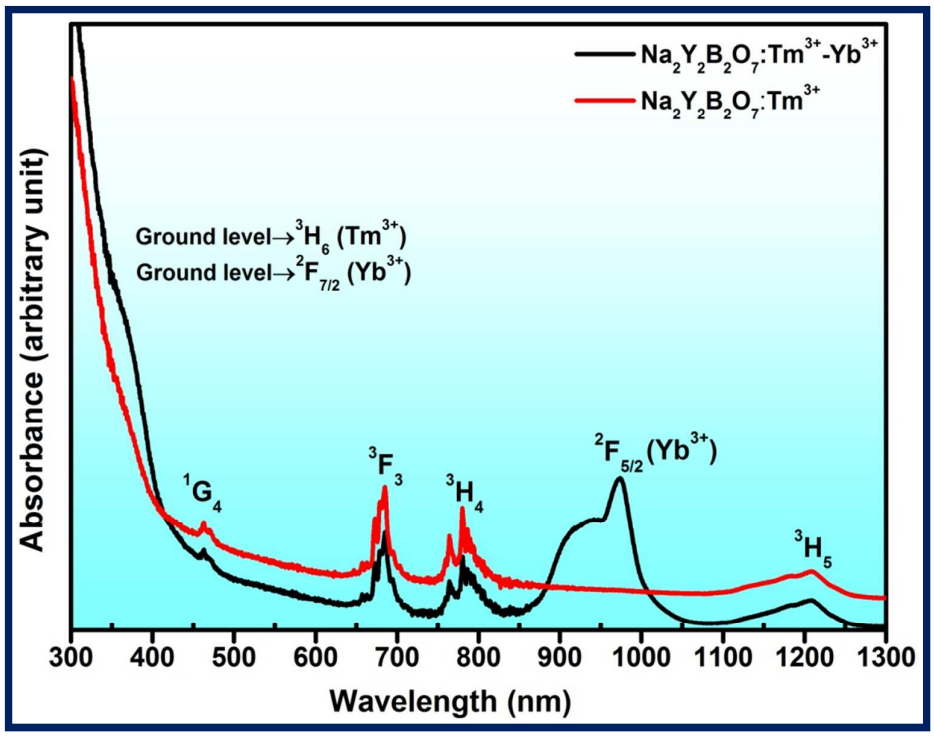

Fig. 4: The absorption spectra for Tm^{3+}/Tm^{3+}-Yb^{3+} doped/codoped $Na_2Y_2B_2O_7$ phosphor in 300-1300nm range.

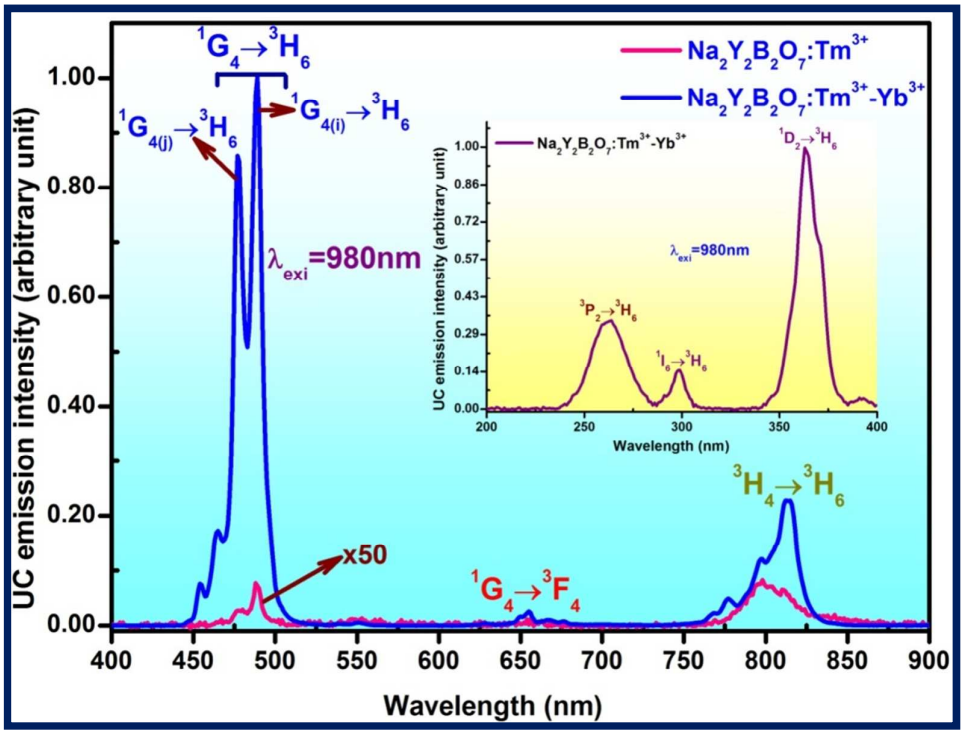

Fig. 5: Comparison of UC emission spectra for Tm^{3+}/Tm^{3+}-Yb^{3+} doped/codoped $Na_2Y_2B_2O_7$ phosphor in 400-900nm range. The inset shows the UC emission intensity spectra for Tm^{3+}-Yb^{3+} codoped $Na_2Y_2B_2O_7$ phosphor in 200-400nm range.

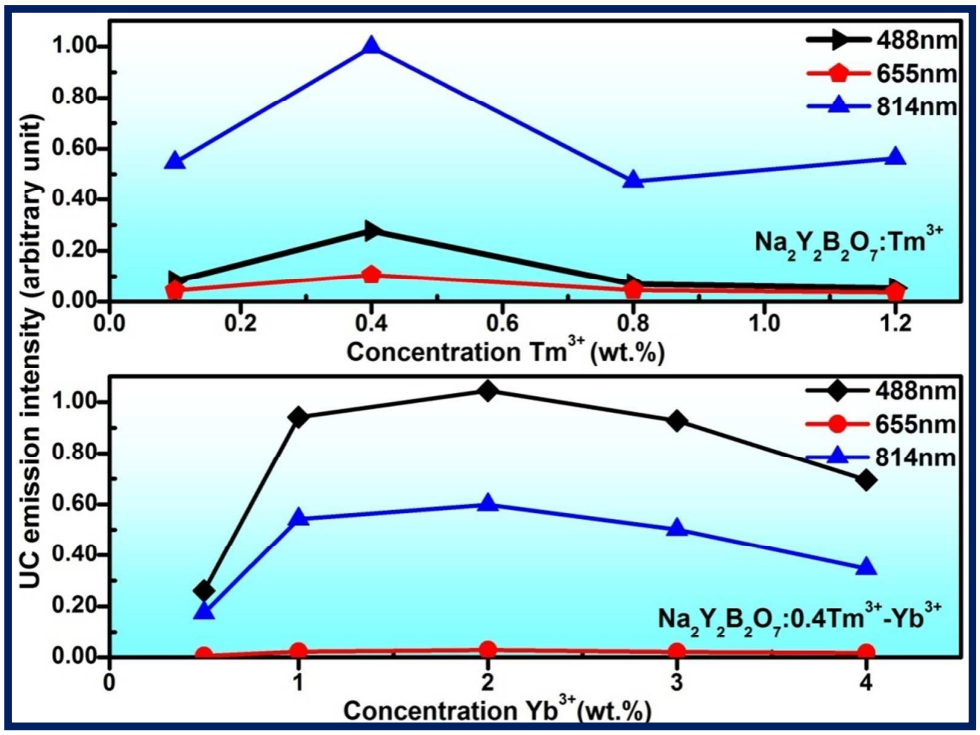

Fig. 6: Dopants (Tm^{3+}, Yb^{3+}) concentration dependence UC emission intensity for $^1G_4 \rightarrow {}^3H_6$ (488nm), $^1G_4 \rightarrow {}^3F_4$ (655nm) and $^3H_4 \rightarrow {}^3H_6$ (814nm) transitions.

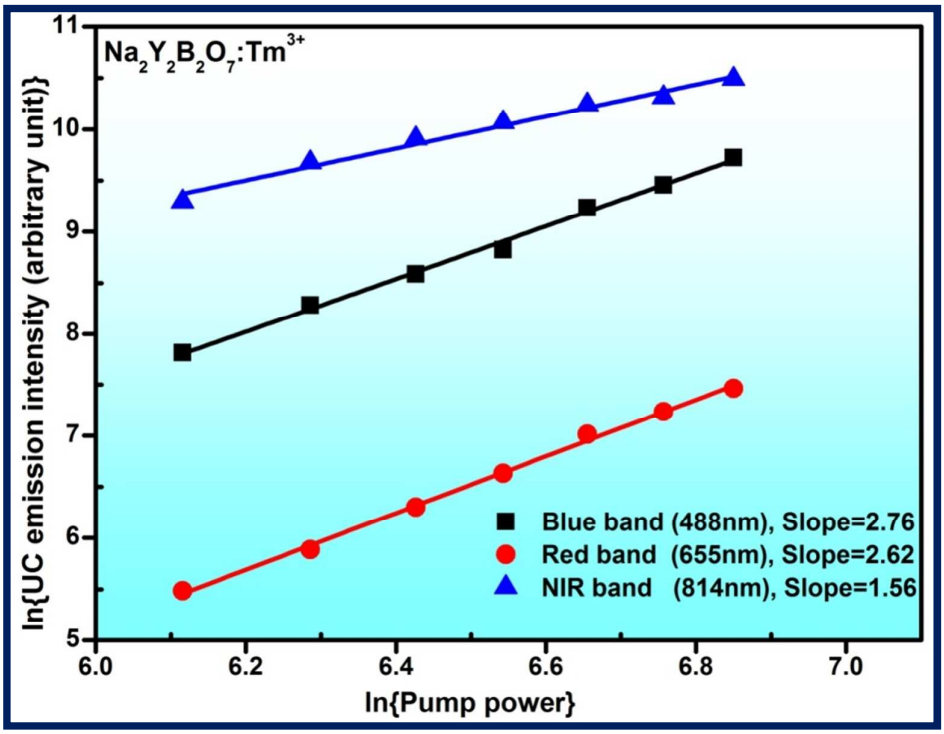

Fig. 7: Pump power dependence study for Tm^{3+} doped $Na_2Y_2B_2O_7$ phosphor.

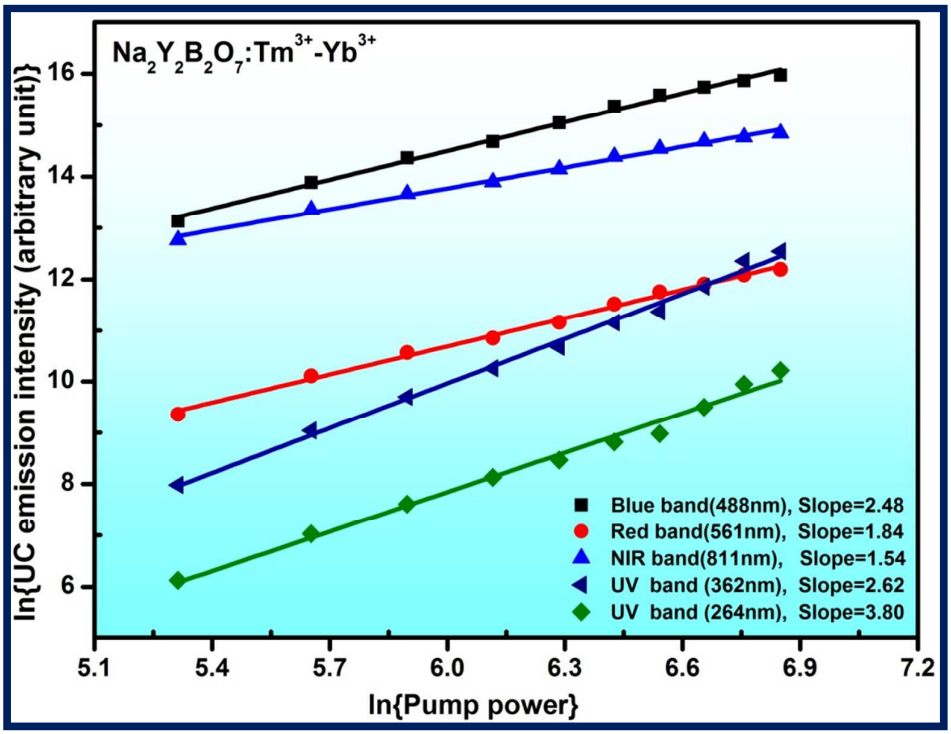

Fig. 8: Pump power dependence study for Tm^{3+}-Yb^{3+} codoped $Na_2Y_2B_2O_7$ phosphor.

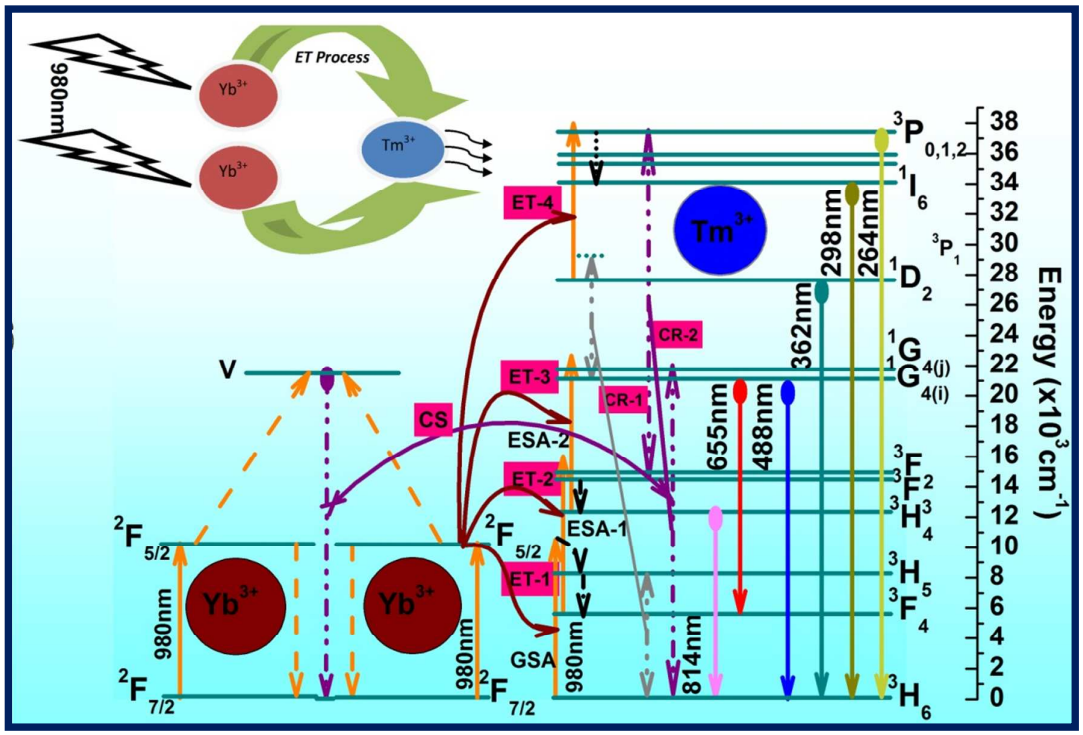

Fig. 9: Schematic energy level diagram for Tm^{3+}-Yb^{3+} codoped $Na_2Y_2B_2O_7$ phosphor.

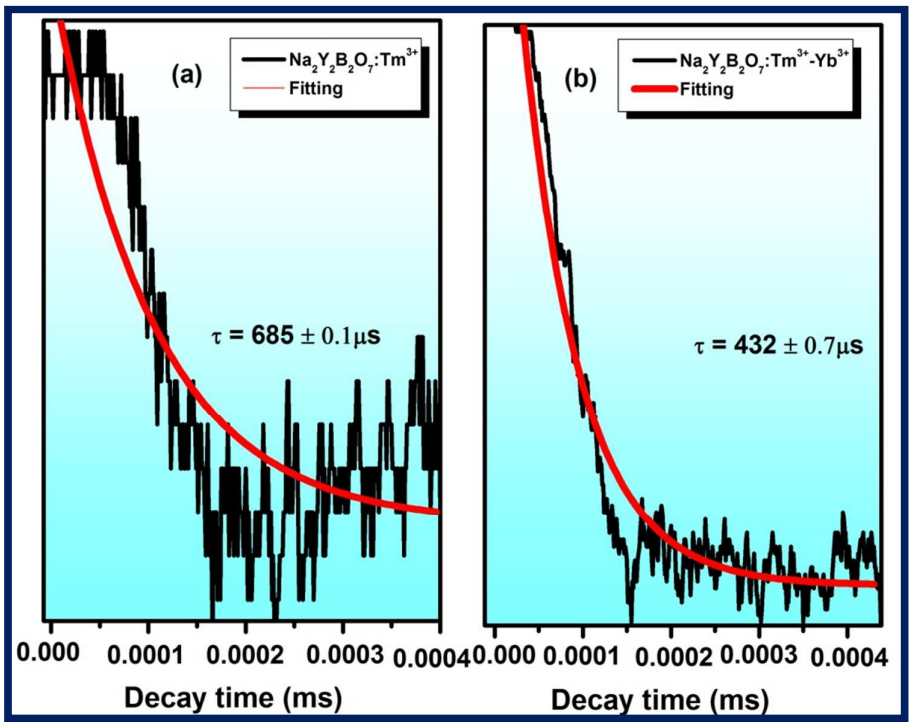

Fig. 10: Decay curve analysis for (a) Tm^{3+} doped $Na_2Y_2B_2O_7$ (b) Tm^{3+}-Yb^{3+} codoped $Na_2Y_2B_2O_7$ phosphor.

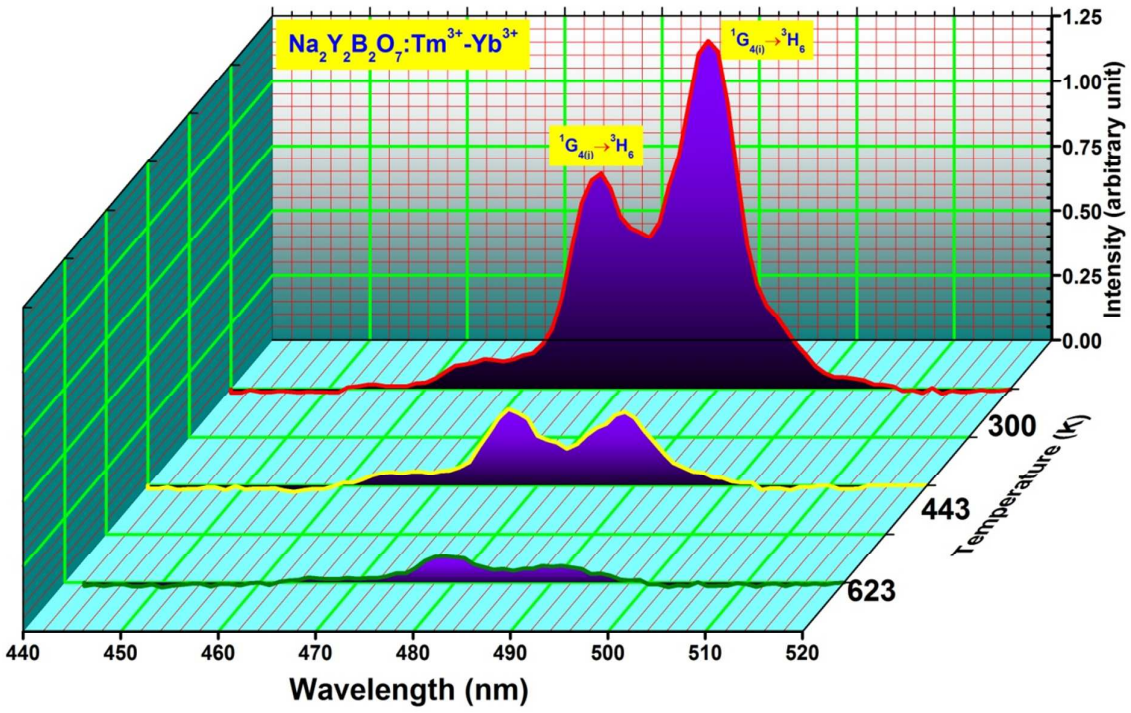

Fig. 11: Blue UC emission spectra of Tm^{3+}-Yb^{3+} codoped $Na_2Y_2B_2O_7$ phosphor in the wavelength range 440-520nm at different temperatures.

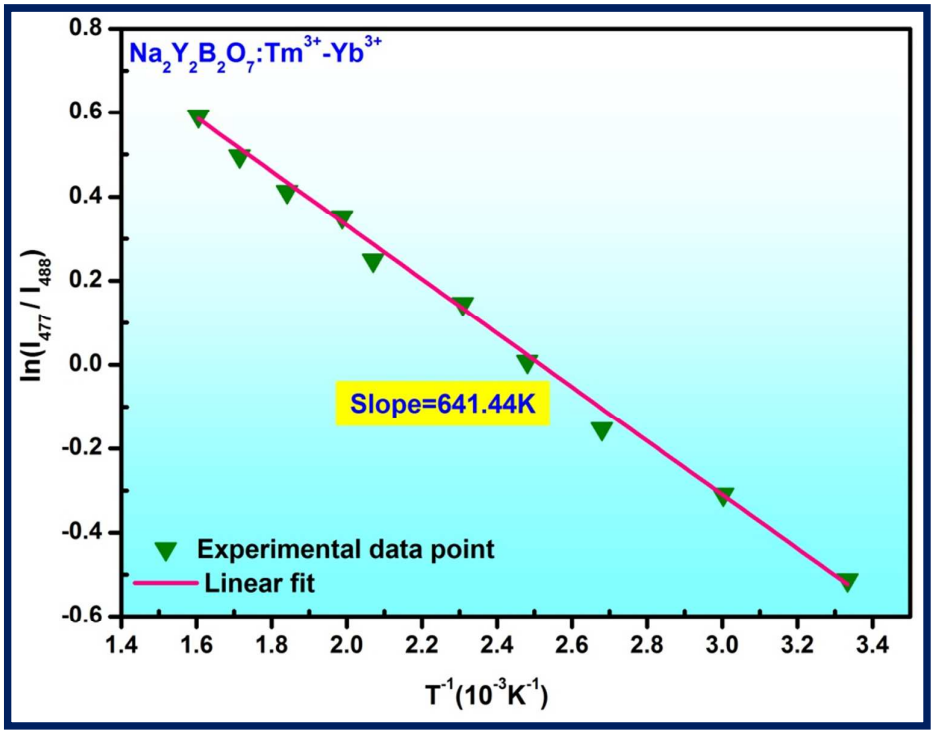

Fig. 12: The plot of monolog FIR versus inverse absolute temperature.

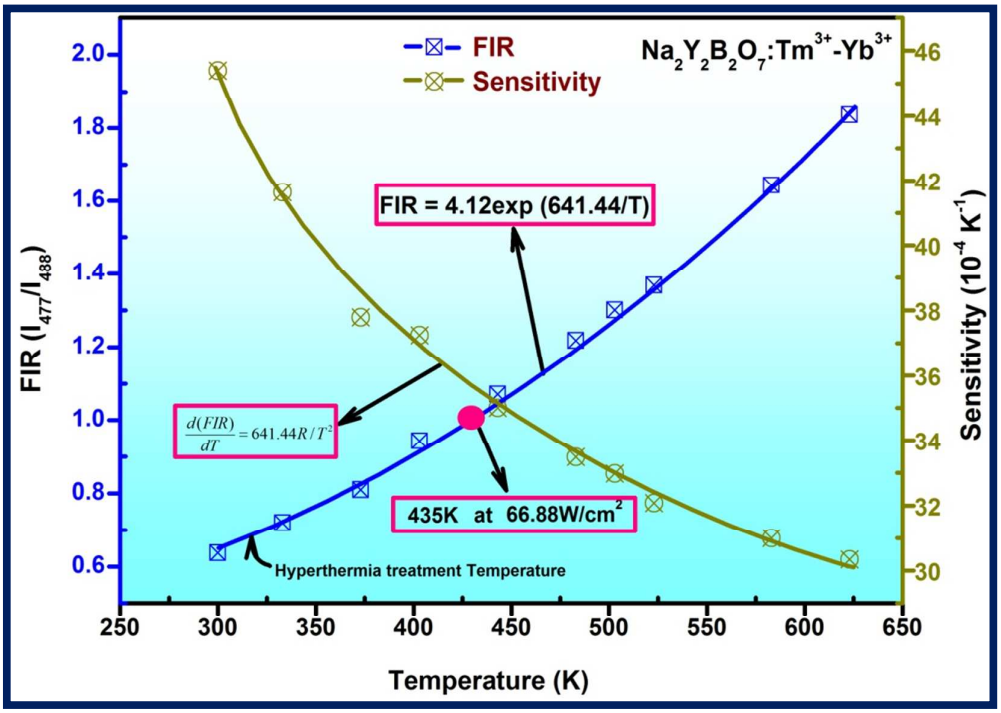

Fig. 13: Variation of FIR and Sensitivity as a function of temperature for Tm^{3+}-Yb^{3+} codoped $Na_2Y_2B_2O_7$ phosphor.

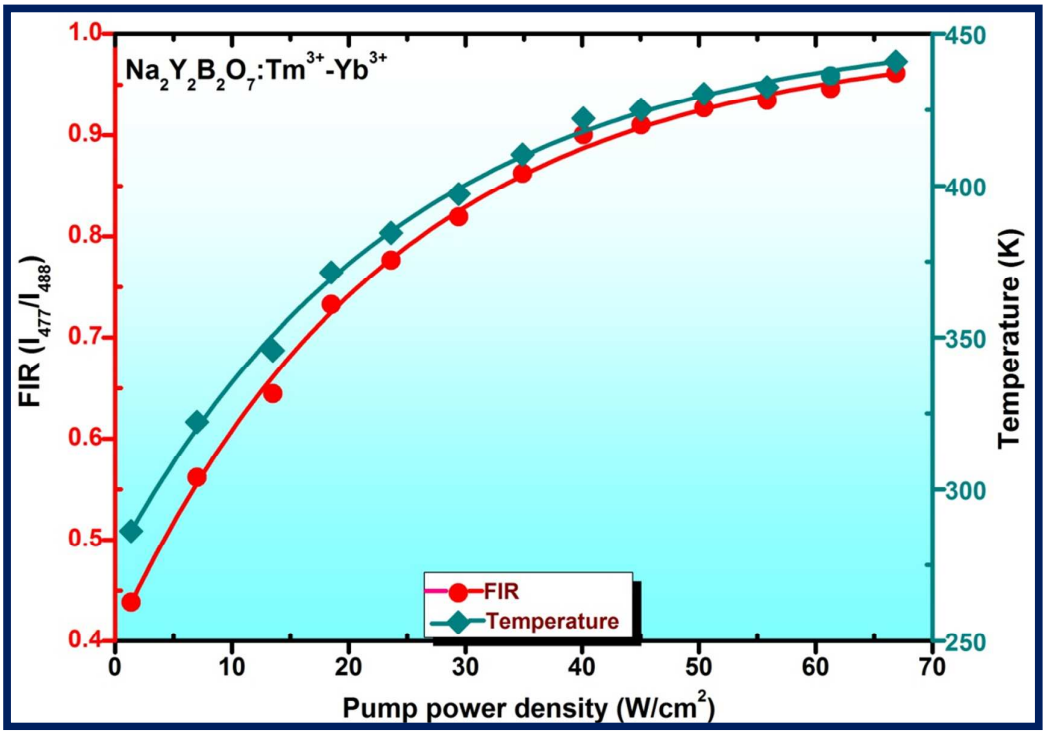

Fig. 14: Variation of FIR and temperature as a function of pump power density for Tm^{3+}-Yb^{3+} codoped $Na_2Y_2B_2O_7$ phosphor.